Smart Structures and Systems, *Vol. 12, No. 5 (2013) 483-499*
DOI:http://dx.doi.org/10.12989/sss.2013.12.5.483

Piezoceramic d_{15} shear–induced direct torsion actuation mechanism: a new representative experimental benchmark

Pelin Berik[1], Ayech Benjeddou[*2] and Michael Krommer[1]

[1]*Institute for Technical Mechanics, Johannes Kepler University, 4040 Linz, Austria*
[2]*Structures, Institut Supérieur de Mécanique de Paris, 93400 Saint Ouen, France*

(Received May 17, 2013, Revised June 23, 2013, Accepted July 1, 2013)

Abstract. A new piezoceramic d_{15} shear-induced torsion actuation mechanism representative benchmark is proposed and its experimentations and corresponding 3D finite element (FE) simulations are conducted. For this purpose, a long and thin smart sandwich cantilever beam is dimensioned and built so that it can be used later for either validating analytical Saint Venant-type solutions or for analyzing arm or blade-based smart structures and systems applications. The sandwich beam core is formed by two adjacent rows of 8 oppositely axially polarized d_{15} shear piezoceramic patches, and its faces are dimensionally identical and made of the same glass fiber reinforced polymer composite material. Quasi-static and static experimentations were made using a point laser sensor and a scanning laser vibrometer, while the 3D FE simulations were conducted using the commercial software ABAQUS®. The measured transverse deflection by both sensors showed strong nonlinear and hysteretic (static only) variation with the actuation voltage, which cannot be caught by the linear 3D FE simulations.

Keywords: piezoceramic d_{15} shear actuation; direct torsion actuation mechanism; piezoelectric composite beam; quasi–static and static experiments; finite element simulation

1. Introduction

Piezoelectric actuators (Niezrecki *et al*. 2001) are nowadays widely used in smart structures and systems. As mono–morphs, they are used in different basic shapes such as tubes, discs and rectangular patches for producing normal (transverse, as stacks), bending (out-of-plane), shear (transverse), twist (in-plane shear induced) or torsion (out-of-plane shear induced) strains. When skewed mono-morph piezoelectric patches can produce bending-twist (Tzou *et al*. 2001) or extension-twist (Finio and Wood 2011) stiffness coupling, they can be used for active twist control (Chopra 2002, Hajianmaleki and Qatu 2013). Twisting actuation can be also reached by anisotropic host composites, having either of the above stiffness couplings, and mono-morph piezoelectric patches (Finio and Wood 2011). As active fiber reinforced composites, piezoelectric actuators, like micro-fiber composite (Choi *et al*. 2007) or macro-fiber composite (Nin and Abramovich 2010, Zehetner *et al*. 2012) patches, with skewed piezoceramic fibers, can produce twisting or torsion actuation due to the induced above stiffness couplings. Instead of skewing the

∗Corresponding author, Professor, E-mail: benjeddou@supmeca.fr

http://www.techno-press.org/?journal=sss&subpage=8 ISSN: 1738-1584 (Print), 1738-1991 (Online)

mono-morph piezoelectric patches or fibers of the composite ones, spiral mono-morph piezoelectric strips (Li *et al*. 2012) or helically electroded piezoceramic hollow or solid fibers (Pan *et al*. 2008) can also produce torsion actuation.

All above twist or torsion actuators, that are based on geometrical or stiffness couplings, use coupled longitudinal (d_{33}) and transverse (d_{31}) piezoelectric response modes; hence, producing twist or torsion likewise is obtained in an indirect manner. Therefore, direct torsion actuation can be obtained using the shear (d_{15}) piezoelectric response (Benjeddou 2007); this generally can be reached by design as suggested numerically by Butz *et al*. (2008) using a two adjacent piezoceramic (PZT–5H) layers composed beam and proved later experimentally (Berik and Benjeddou 2010) and numerically (Benjeddou 2011) using a sandwich plate actuator made of axially oppositely poled (OP) two adjacent rows of triple PZT PIC255 patches and glass fiber reinforced polymer (GFRP) faces. Both configurations were analyzed in statics. The latter torsion actuation mechanism (TAM), as studied in Berik and Benjeddou (2010) and in Benjeddou (2011), is further analyzed here by conducting new quasi-static and static experiments for a new benchmark; the latter consists of a thin and long sandwich cantilever beam made of a segmented piezoceramic core, that is assembled from 16 patches which are arranged in two rows of 8 oppositely *axially polarized* patches each, and of two identical GFRP faces; the benchmark is representative in the sense that it is dimensioned such that it can be useful for validating Saint Venant–type analytical solutions (Krommer *et al*. 2012, 2013) and for proving blade- or arm-based smart concepts for rotorcrafts, wind turbines and robotics for example.

Compared to the authors' previous works on the sandwich *plate*-like experimental benchmark *static* torsion actuation testing using *Electronic Speckle Pattern Interferometry* (ESPI) system (Berik and Benjeddou 2010) and 3D finite element (FE) analysis (Benjeddou 2011), and on mono-morph (Krommer *et al*. 2012), bimorph and sandwich (Krommer *et al*. 2013) beam-like Saint Venant - type analytical solutions of the direct d_{15} shear-induced TAM, the present one contributes originally with:

- New sandwich *beam*-like experimental benchmark and corresponding *quasi-static* and static tests using point and scanning *laser* sensors; previously only static actuation of a sandwich plate benchmark was conducted using an ESPI system;
- *Quasi-static* experimental tests and their FE analysis; they showed only experimental difference with the static ones since *ABAQUS® coupled piezoelectric FEs have not any nonlinearity*;
- Experimental *visualization* of the d_{15} shear-induced *3D torsion deformation* through the quasi-static scanning laser deflection measurements; in earlier works, this was achieved only through 3D FE analysis;
- Experimental *proof* of the d_{15} shear-induced TAM through the cantilever tip left and right edges quasi-static actuation *phases* comparison and *displacements overlapping*;
- Experimental *proof* of the *hysteresis* presence during static torsion actuation only; no hysteresis was observed for quasi-static actuation; the hysteresis phenomenon has not been investigated earlier for the direct d_{15} shear induced TAM.
- Reference *tabulated* experimental quasi-static and static deflection and rate-of-twist results under loading and *un-loading* different actuation voltages; this served, for example, for experimentally validating the Saint Venant–type analytical solution (Krommer *et al*. 2013);

Hereafter, the proposed experimental benchmark and conducted quasi-static and static tests are first described; then, the corresponding experimental results are discussed, and 3D FE simulations

are described and corresponding results are compared to the experimental ones. Finally, some conclusions and perspectives are given as a closure.

2. Experimental benchmark and tests

The proposed new experimental benchmark for the TAM response characteristics quasi–static and static analyses consists of a piezoelectric smart beam made of a piezoceramic core (Fig. 1(a)) that is sandwiched between two identical GFRP composite faces (Fig. 1(b)). The core is assembled adhesively from 16 axially polarized d_{15} shear PZT PIC255 (PI Germany) patches, of dimensions $25\times10\times0.5$ mm^3 each and arranged in two adjacent rows composed of 8 OP patches, while the faces are made of Polyspeed G-EW 760R glass fiber reinforced polymer (epoxy) composite layers (Hexcel Austria), of dimensions $200\times20\times0.5$ mm^3 each. The non–conducting glue is spread only on the patches upper and lower faces; hence, adhesive layers can be assumed present only at the sandwich interfaces, while vertical interfaces are not glued in order to avoid contacting the patches top and bottom electrodes. Electrically, the lower electrodes are grounded; mechanically, the sandwich beam is cantilevered.

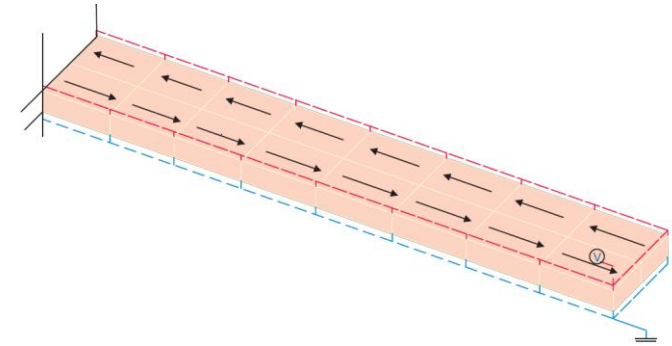

(a)

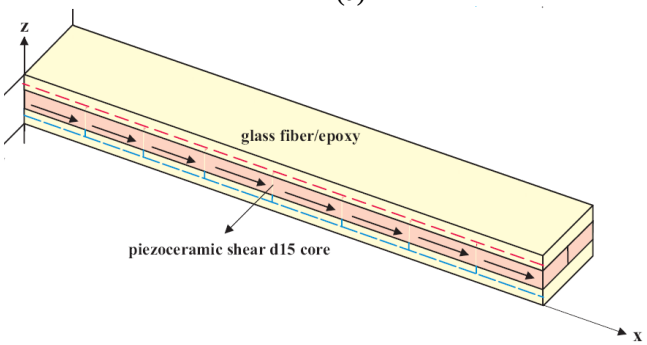

(b)

Fig. 1 (a) Sketches of the piezoceramic d_{15} shear patches assembled core and (b) experimental beam benchmark

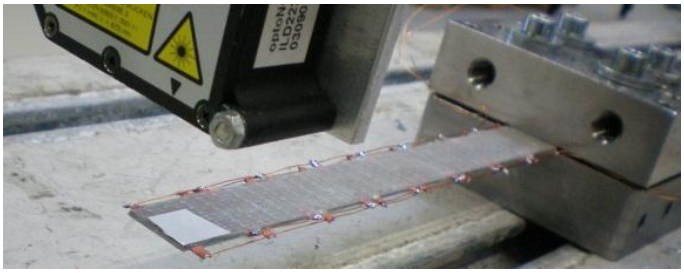

(a)

(b)

Fig. 2 Photos of the smart beam benchmark during torsion actuation experiments conducted by a laser displacement sensor (a) in quasi–statics (1 Hz) and statics, and by a laser scanning vibrometer (b) in quasi–statics (2 Hz)

2.1 Quasi–static torsion actuation experiment set-ups

The quasi–static torsion actuation experiments are carried out on the cantilever piezoelectric smart sandwich beam benchmark by applying different AC voltages ranging from 35 V to 195 V at 1 Hz for the measurements using a point laser displacement sensor (Micro–Epsilon laser sensor of type Opto–NCDT 2220, Fig. 2(a)) and 2 Hz for those using the scanning laser vibrometer (PSV–400 Polytec laser scanning vibrometer, Fig. 2(b)) to the piezoceramic torsion core in order to detect the smart beam tip maximum transverse displacement from which the rate-of-twist is post–processed.

The cantilever smart sandwich beam's tip maximum rate-of-twist, α^{max}, for both quasi–static and static torsion actuation experiments is post-processed using the relation

$$\alpha^{max} = \frac{2u_z^{max}}{Lb} \tag{1}$$

where, $u_z^{\max}$, L and b are the maximum tip transverse deflection and the length and width of the beam, respectively.

The other test equipment used in the experiments are an Agilent power supply (type E3611A), Dewetron high voltage isolator module (type DAQN-DMM), a PI high voltage amplifier (type HVPZT) and a pulse multi–analyzer system (Brüel & Kjaër with input/output module type 3109 and LAN interface module type 7533).

Flowcharts of the performed quasi–static torsion actuation experiments are shown in Fig. 3.

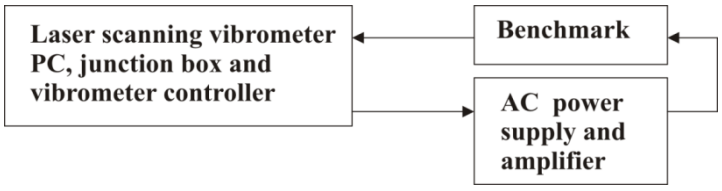

(a)

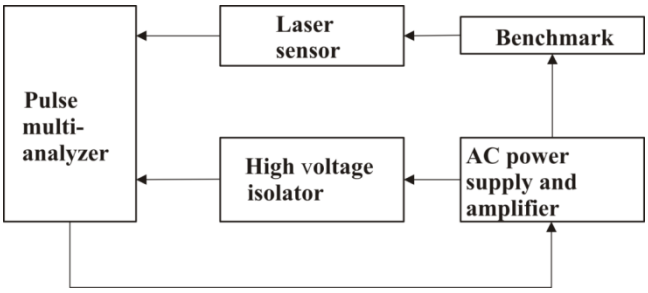

(b)

Fig. 3 Flowcharts of the experimental set-ups using a laser scanning vibrometer (a) and a laser displacement sensor (b) for quasi-static (with AC power supply) actuation experiments

2.2 Static torsion actuation experiment set-up

As shown in Fig. 4(a), the static torsion actuation experiments, performed using the point laser displacement sensor with the static laser light (Fig. 4(b)), have the same experimental set-up as the quasi-static one, with the exception that the applied voltage source is of DC type this time.

Static torsion actuation experiments are executed by detecting first the initial free–end–tip position of the benchmark by the point laser displacement sensor at 0 V and then applying a DC voltage; as the next step, the new free–end–tip position of the benchmark is measured. Then, the relative displacement is post-processed; subsequent DC voltage deflections are calculated in the same manner. This procedure is repeated for both the left and the right side of the benchmark.

The static measurements are performed using the laser sensor by applying DC voltages ranging from 36.87 V to 188.54 V to the core of the smart sandwich beam benchmark. Due to the well-known capacitive nature of piezoceramics, the piezoceramic core is short-circuited before conducting these static experiments in order to annihilate any possible retained strain.

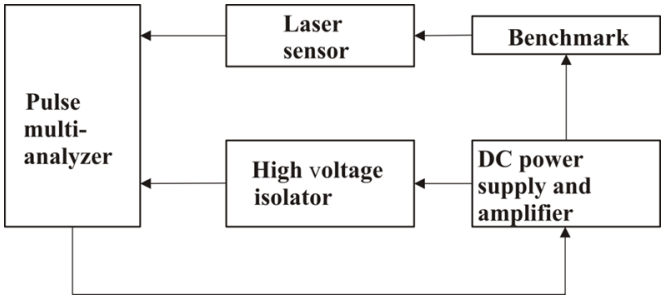

(a)

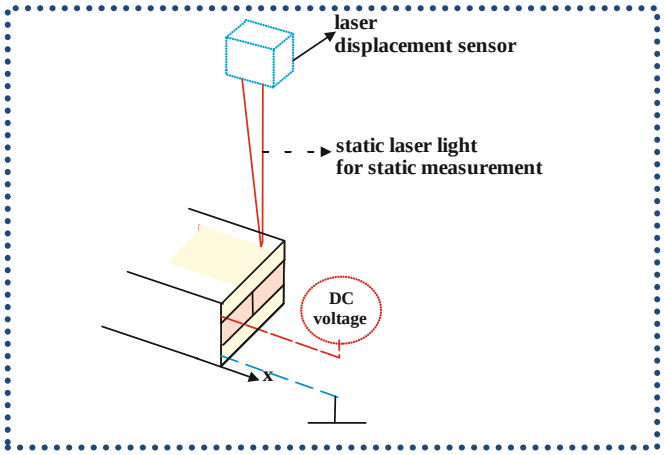

(b)

Fig. 4 Flowchart (a) and position of the laser displacement sensor with static laser light (b) of the experimental set-up for the static (with DC power supply) torsion actuation experiments

3. Experimental results

3.1 Quasi–static torsion actuation

Fig. 5(a), which is obtained by the point laser sensor, shows the auto-spectrum of the transverse displacement of the smart sandwich beam benchmark on the right edge of the free side for quasi-statically (at 1 Hz) actuating torsion by applying a voltage of 191.08 V. The transverse tip deflection measurements are executed for both, the left and the right side of the free end of the benchmark and the mean beam transverse tip deflection at this actuation voltage is 12.862 µm. The voltage auto-spectrum for these measurements is presented in Fig. 5(b). In order to obtain the actual transverse deflection and applied voltage values, the auto-spectrum values must be multiplied by the square root of 2.

Fig. 6, which is obtained by the laser scanning vibrometer, shows the global twist deformation (a), transverse deflection distribution on the surface (b), and its variation along the tip cross section width (c) of the benchmark for quasi-statically (at 2 Hz) actuating torsion by applying a voltage of

195 V. It's worthy to notice that this experimental 3D global torsion deformation (Fig. 6(a)), visualized thanks to the scanning laser vibrometer, is shown here for the first time. Earlier illustrations, as in Figs. 6(a), 6(b) and 6(c), were obtained only numerically through FE simulations (Butz *et al*. 2008, Berik and Benjeddou 2010, Benjeddou 2011).

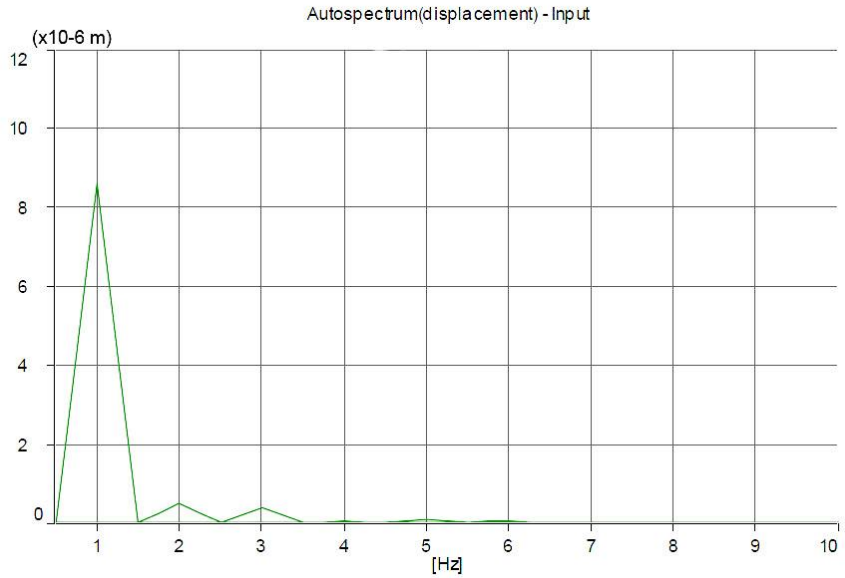

(a)

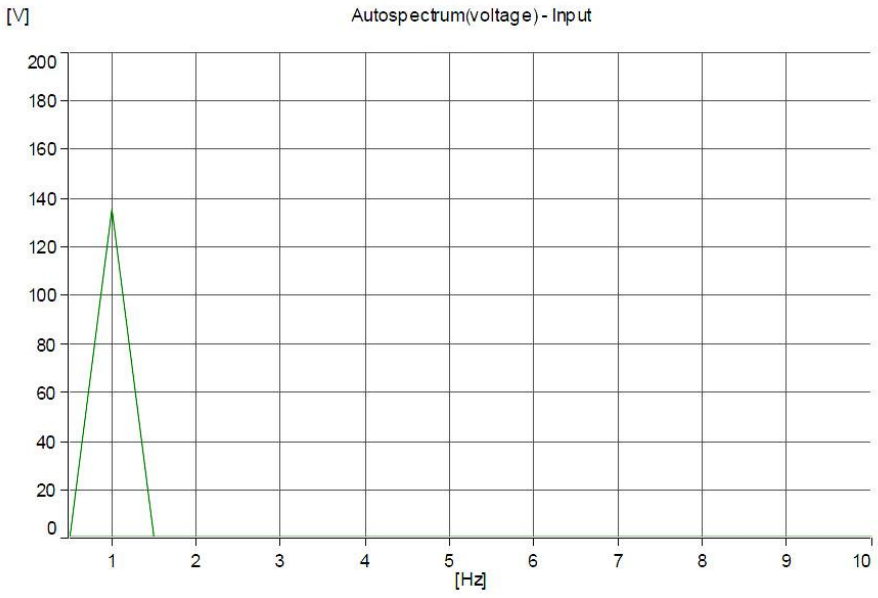

(b)

Fig. 5 Transverse displacement auto-spectrum at 191.08 V (a) and voltage auto-spectrum at 191.08 V (b) during the quasi-static (1 Hz) torsion actuation experiments using the point laser sensor

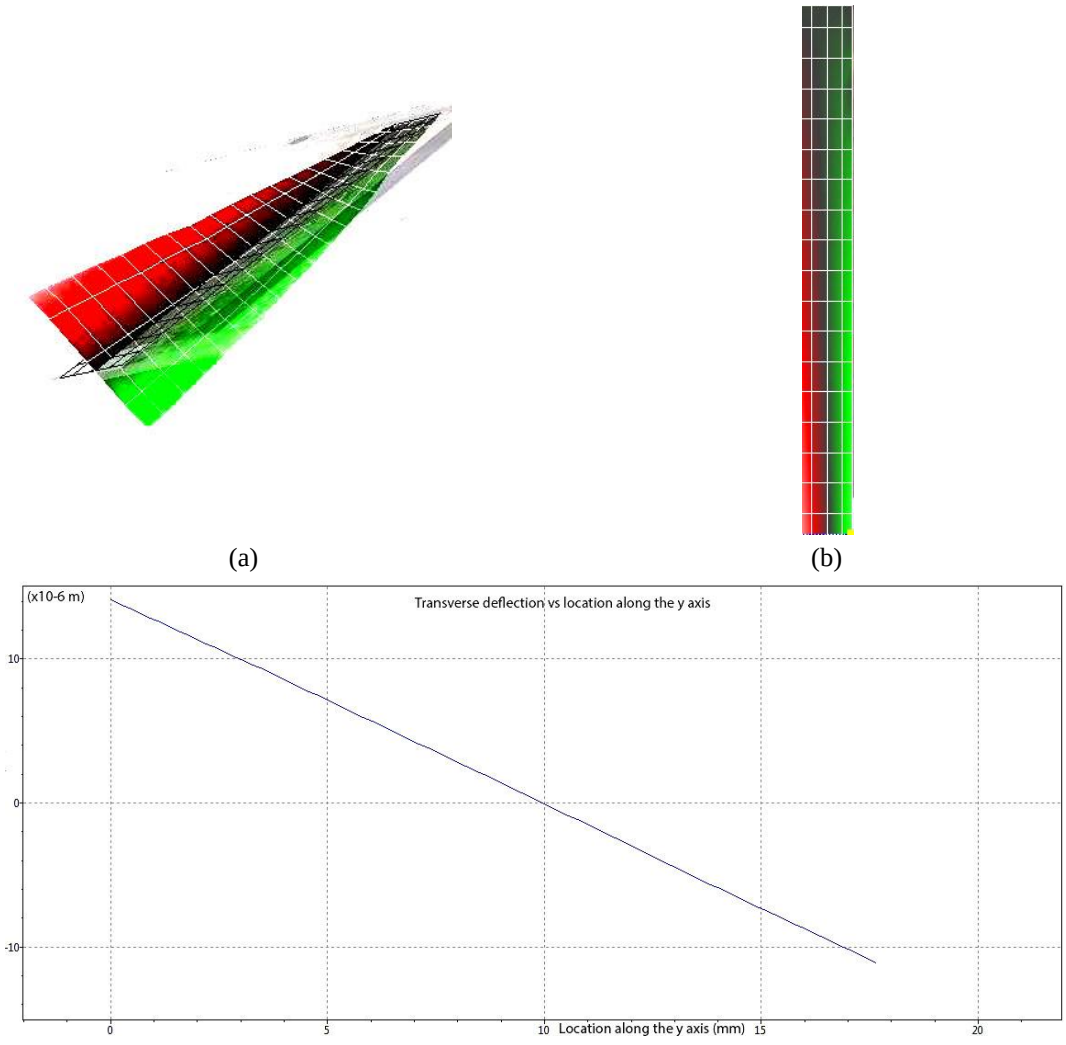

Fig. 6 The laser scanning vibrometer measured global twist deformation (a), transverse deflection surface distribution (b) and transverse deflection variation along the cross section width (c) of the benchmark during the quasi-static torsion actuation experiments (195 V at 2 Hz)

The displacement-voltage cross-spectrum phase curves of the left and right edges of the free side of the smart sandwich beam are shown in Fig. 7. It must be noted that there is an approximately 180° phase difference between these two curves. This phase difference is expected and can be seen as a proof of the torsion actuation concept since the left and right parts of the piezoceramic core have OP directions.

The overlapped time-voltage and displacement curves for the right and left edges of the free side of the smart beam are given in Fig. 8. The phase difference between overlapped displacement curves can also be noticed for the right and left sides of the beam benchmark in this figure.

The results obtained from quasi-static torsion actuation experiments are presented in Table 1. Meanwhile, it must be indicated that the measurements using the point laser sensor and the scanning laser vibrometer have not been performed exactly at the same applied voltages because the voltage source was a manual type and it was not possible to arrange the exact application of the same voltage values. For this reason, the measured transverse deflections and post-processed rates-of-twist values are divided by the applied voltage so that corresponding per volt values are taken as the main comparison criterion for the TAM performance assessment.

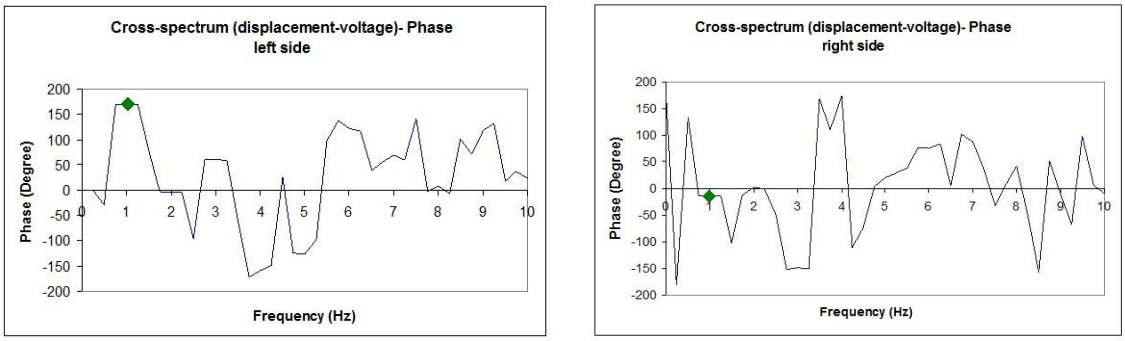

(a) (b)

Fig. 7 Displacement–voltage cross–spectrum phase curve of the left edge (a) and right edge (b) of the free side of the beam during torsion actuation experiments with the laser sensor at quasi-static voltage of 191.08 V at 1 Hz

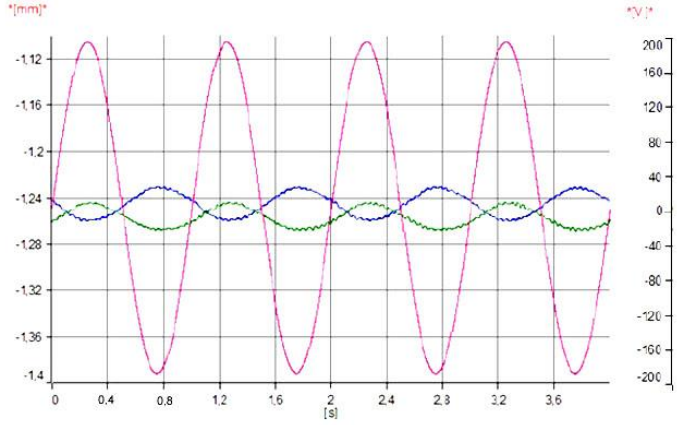

Fig. 8 Overlapped voltage-time (red) and displacement-time curves for the right (blue) and left (green) edges of the smart sandwich beam free side during the torsion actuation experiments with the laser sensor at a quasi-static (1 Hz) voltage of 191.08 V (the voltage scale is on the right side and that of the displacements is on left one

From Table 1, it can be observed that quasi-static actuation experiment results using the laser sensor and the laser scanning vibrometer are similar for similar applied voltages; but, the rate-of-twist per volt and the transverse deflection per volt values at applied voltages near 190 V and 150 V show some differences that can be attributed to the nonlinear piezoceramics actuation response as can be seen hereafter from the maximum tip transverse displacement variation with the actuation voltages.

Table 1 Measured transverse deflections per volt and post-processed rates-of-twist per volt values for quasi-static torsion actuation experiments using the point laser sensor (at 1 Hz) and the scanning laser vibrometer (at 2 Hz)

Post-processed/measured quantity (unit) Sensor (applied voltage at frequency)	Rate-of-twist per volt (10^{-6} $V^{-1}m^{-1}$)	Transverse deflection per volt (nm/V)
Point Laser (191.08 V at 1 Hz)	33.656	67.312
Scanning Laser (195 V at 2 Hz)	34.397	68.785
Point Laser (150.03 V at 1 Hz)	30.774	61.548
Scanning Laser (150.03 V at 2 Hz)	31.187	62.373

3.2 Static torsion actuation

The static experimental cantilever smart sandwich beam transverse deflections per volt curves and their comparison to the quasi-static ones obtained by the laser sensor and the laser scanning vibrometer loading and unloading voltages are shown in Fig. 9.

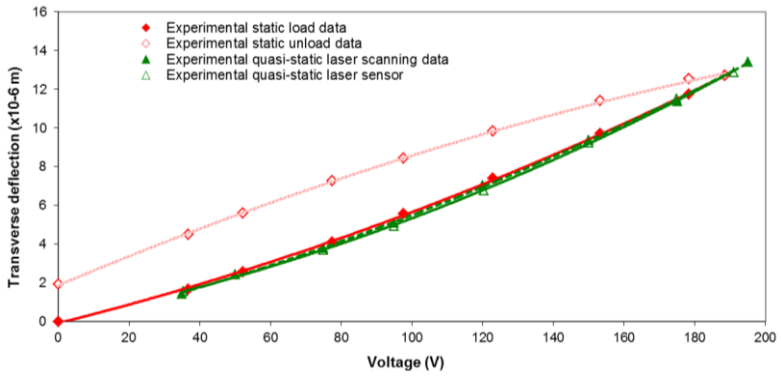

Fig. 9 Experimental static (with hysteresis) and quasi-static actuation load– and unload–induced transverse deflections

It can be noticed from Fig. 9 that all experimental results show nonlinear quasi-static and static responses. However, in contrary to the static measurements, the quasi-static torsion actuation experiments do not show any noticeable hysteresis, neither using the point laser sensor nor using the scanning laser vibrometer. A residual strain can be also noticed at unloading 0 V actuation. This hysteretic non linear static torsion actuation response and the corresponding residual strain at unloading 0 V actuation were also observed by others for static indirect torsion (Pan *et al*. 2008) and transverse (Yocum and Abramovich 2002) actuation responses.

Some rate-of-twist per volt and transverse displacement values from Fig. 9 are given in Table 2 for future reference. Worthy to notice that in this table, and as can be seen in Fig. 9, 188.54 V is the maximum applied voltage in static torsion actuation experiments, and, from this single point the voltage was started to be reduced; for this reason, there is no unload value for 188.54 V in Table 2.

Table 2 Rates-of-twist per volt and transverse deflections per volt values for load and unload static torsion actuation experiments using the point laser sensor

Post-processed/measured quantity (unit) Static (applied voltage)	Rate-of-twist per volt (10^{-6} $V^{-1}m^{-1}$)	Transverse deflection per volt (nm/V)
Load (188.54 V)	33.653	67.307
Load (153.24 V)	31.686	63.371
Unload (153.24 V)	37.206	74.413

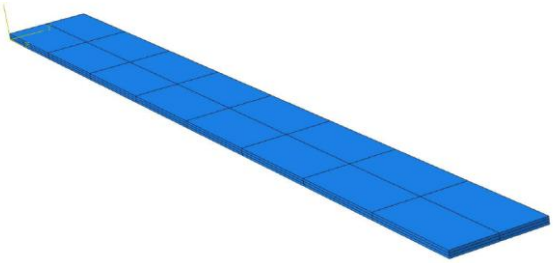

(a)

(b)

Fig. 10 Geometric 3D model (a) and corresponding FE mesh (b) of the smart sandwich beam

4. Finite element simulations of the experimental benchmark

The 3D geometric (Fig. 10(a)) and FE (Fig. 10(b)) models are made using ABAQUS® commercial code. They can take, or not, into account the interface adhesive layers (assumed to have a uniform thickness of 0.1 mm each) between the piezoceramic core and the GFRP composite faces. Corresponding FE meshes have 2 elements through the thickness of the piezoceramic layers and 1 element through the thickness of the GFRP composite faces and adhesive layers at the smart sandwich beam interfaces. All layers have 200 elements along their length and 20 elements along their width, leading to a total of 16,000 elements and 79,089 nodes for the model without (w/o) adhesive layers, and 24,000 elements and 120,855 nodes for that with adhesive layers. The materials properties are recalled from Berik and Benjeddou (2011) in Table 5 of Appendix A. The 3D FE simulations were made under both static and quasi-static options. The smart sandwich beam maximum rate-of-twist is post-processed from its tip maximum transverse displacement using Eq. (1).

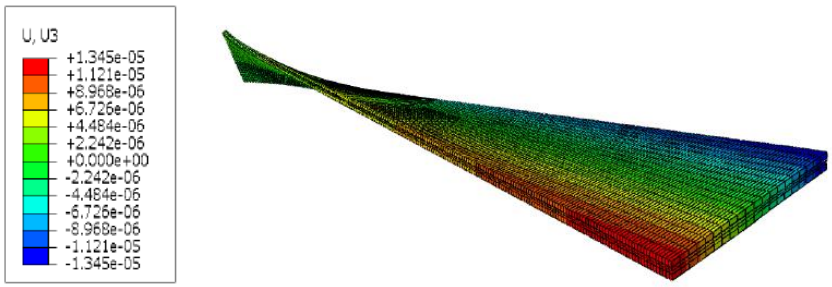

(a)

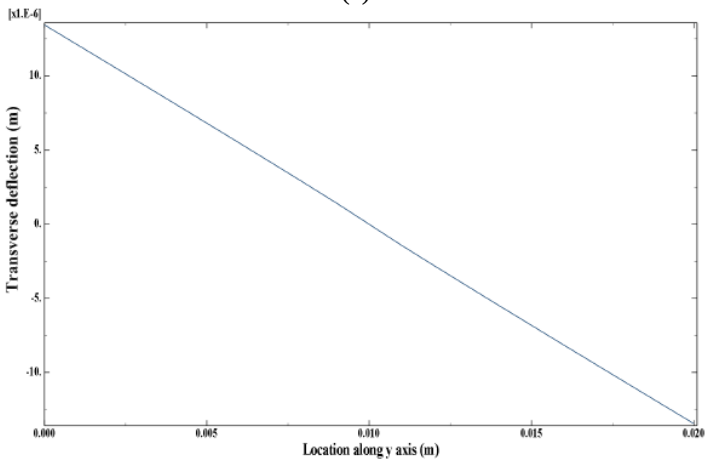

(b)

Fig. 11 FE simulated global twisting deformation of the benchmark (a) and its transverse deflection variation along the tip cross section (b) under quasi-static actuation at 195 V

The simulated global twist deformation and corresponding transverse deflection variation along the tip cross section under 195 V quasi-static torsion actuation are shown in Figs. 11(a) and 11(b), respectively; it can be observed that simulated (Fig. 11) and experimental (Fig. 6) results are qualitatively similar. Quantitatively, since the quasi-static and static 3D FE simulation results were found to have the same transverse deflection values for the same actuation voltages, only the quasi-static FE results, w/o and with modeling the sandwich interlayer adhesives, are compared to the experimental static and quasi-static ones in Tables 3 and 4, before and after dividing the results by the actuation voltages. It is worthy to recall that the static experiments show the results obtained with the laser sensor, while the quasi-static ones show those obtained with the scanning laser vibrometer. Also, as said earlier, since the voltage source was a manual type, it was not possible to arrange the exact application of the same voltage values; for this reason, in these tables, quasi–static and static experiments do not have exact matching voltage values sometimes.

Table 3 Comparisons of the rate-of-twist and transverse deflection values of the quasi-static 3D FE simulations w/o and with adhesive layers to experimental results (static experiments with the point laser sensor, quasi-static ones with the scanning laser vibrometer)

Quantity		Rate-of-twist (10^{-3} m^{-1})			Transverse deflection (μm)		
Actuation voltage		150 V	188.54 V	195 V	150 V	188.54 V	195 V
Quasi–static 3D FE simulations	w/o adhesives	5.173	6.502	6.725	10.346	13.004	13.450
	with adhesives	4.531	5.695	5.890	9.061	11.390	11.780
Experiments	Static		6.345			12.690	
	Quasi–static	4.678		6.707	9.356		13.415

Table 4 Comparisons of the rate-of-twist *per volt* and transverse deflection *per volt* values of the quasi-static 3D FE simulations w/o and with adhesive layers to experimental results (static experiments with the point laser sensor, quasi-static ones with the scanning laser vibrometer)

Quantity		Rate of twist *per volt* (10^{-6} V^{-1} m^{-1})			Transverse deflection *per volt* (nm/V)		
Actuation voltage		150 V	188.54 V	195 V	150 V	188.54 V	195 V
Quasi–static 3D FE simulations	w/o adhesives	34.487	34.487	34.487	68.974	68.974	68.974
	with adhesives	30.205	30.205	30.205	60.410	60.410	60.410
Experiments	Static		33.653			67.307	
	Quasi–static	31.187		34.397	62.373		68.785

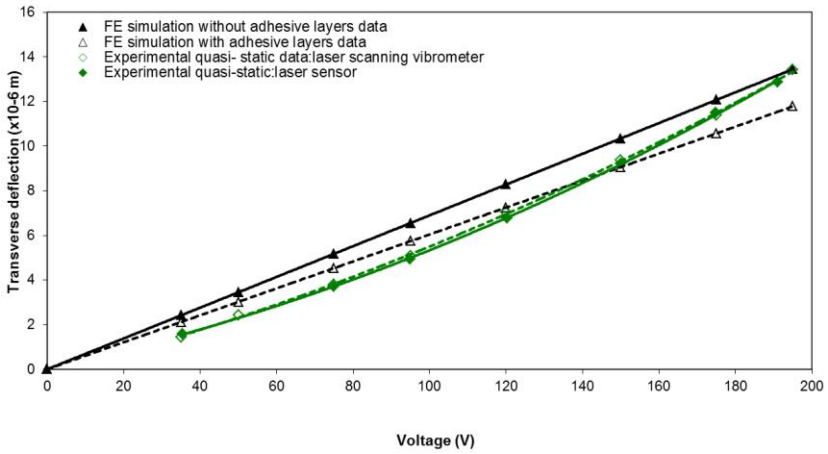

Fig. 12 3D FE simulated and experimental transverse deflection variations with quasi-static actuation voltages

From Tables 3 and 4, it can be noticed that the adhesives effect depends on the actuation voltage; that is, the simulation results with adhesives are closer to the experimental ones at low actuation voltages, while those w/o adhesives are closer to the experimetal ones at higher voltages. Also, the quasi-static 3D FE simulations are closer to the static experimental results at low actuation voltages and to the quasi-static ones at high actuation voltages. These behaviors are due to the quasi-static and static torsion actuation nonlinear experimental responses as can be noticed from Figs. 12 and 13 showing, respectively, the cantilever smart sandwich beam transverse deflection and rate-of-twist variations with the actuation voltages. Naturally, the linear quasi-static 3D FE simulations are not able to catch such non linearity since ABAQUS® coupled piezoelectric FEs have only linear modelling and simulation capability.

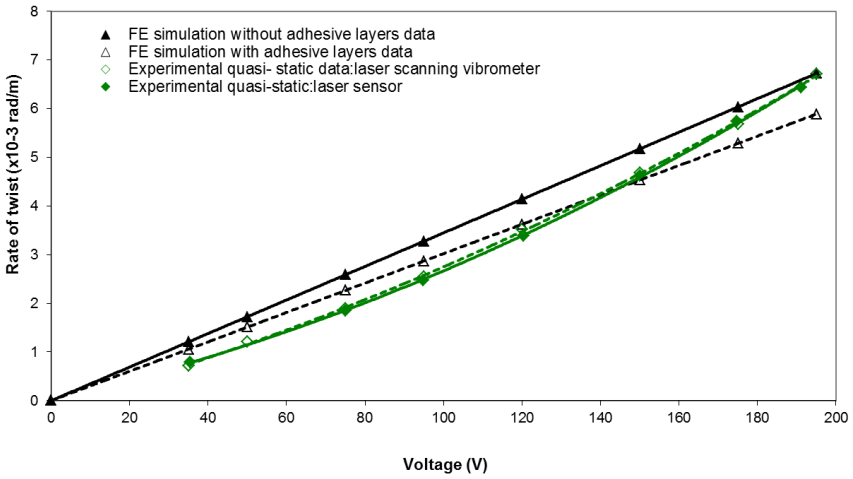

Fig. 13 3D FE simulated and experimental *rate-of-twist* variations with quasi-static actuation voltages

5. Conclusions

A new experimental benchmark has been proposed for the analysis of the quasi-static and the static response of the piezoceramic d_{15} shear–induced direct torsion actuation mechanism (TAM).

It consists of a long and thin smart sandwich cantilever beam with a piezoceramic core, assembled from 16 patches that are arranged in two segmented rows of two pairs of 8 oppositely axially polarized patches, and glass fiber reinforced polymer composite faces. For the analysis of the TAM response characteristics, the benchmark experiments were conducted under varying quasi-static and static actuation voltages. For this purpose, the cantilever smart sandwich beam tip transverse deflections were measured by a point laser sensor, in quasi-statics and statics, and by a scanning laser vibrometer in quasi-statics; the corresponding 3D finite element (FE) simulations were also made under the same conditions. The rates-of-twist were then post–processed from the obtained experimental and numerical deflections; finally, all results were divided by the actuation voltages for the assessment of the TAM performance.

The 3D global twisting deformation and corresponding transverse displacement linear variation through the tip cross-section width, obtained by the FE simulation, were proved for the first time qualitatively by the scanning laser vibrometer quasi-static torsion actuation experiments. Besides, in contrary to the quasi-static point and scanning laser sensors measurements, the point laser sensor static torsion actuation experiments showed a strong hysteretic response with a noticible residual strain at 0 V unloading voltage; this issue was investigated here for the first time.

However, both quasi-static and static measurements showed a strong nonlinear response, which cannot be caught by the linear 3D FE simulations since ABAQUS® available coupled piezoelectric FEs do not implement any non linearity. The corresponding experimental tabulated data can serve for evaluating future extensions of both analytical and numerical simulations with respect to the observed electric field dependent and hysteritic non-linear responses.

As an immediate continuation of the present work, sensing experiments and corresponding 3D FE simulations were conducted (Chevallier *et al*. 2013). Also, analytical Saint Venant–type solutions were developed for a continuous piezoceramic torsion actuation core (Krommer *et al*. 2012) and for the present smart sandwich beam benchmark (Krommer *et al*. 2013). Research on dynamic sensing and actuation experiments, and corresponding simulations and analytical modeling are in progress, while the electric field dependent non linear response modeling and simulation remain open issues.

Acknowledgments

The authors gratefully acknowledge the support of the present research by the peer reviewed Comet-K2 Austrian Centre of Competence in Mechatronics (ACCM) at Linz, Austria.

References

Benjeddou, A. (2007), "Shear-mode piezoceramic advanced materials and structures: a state of the art", *Mech. Adv. Mater. Struct.*, **14**(4), 263-275.

Benjeddou, A. (2011), "Assessment of a smart concept for d_{15} shear piezoceramic direct torsion actuation", *Eur. J. Computational Mech.*, **20**(1-2-3), 103-123.

Berik, P. and Benjeddou, A. (2010), "Piezoelectric d_{15} shear response–based torsion actuation mechanism: an experimental benchmark and its 3D finite element simulation", *Int. J. Smart Nano Mater.*, **1**(3), 224-235.

Berik, P. and Benjeddou, A. (2011), "Static experimentations of the piezoceramic d_{15}–shear actuation mechanism for sandwich structures with opposite or same poled patches–assembled core and composite faces", *Int. J. Smart Nano Mater.*, **2**(4), 230-244.

Butz, A., Klinkel, S. and Wagner, W. (2008), "A geometrically and materially non–linear piezoelectric three-dimensional beam finite element formulation including warping effects", *Int. J. Numer. Meth. Eng*., **76**(5), 601-635.

Chevallier, G., Berik, P., Benjeddou, A. and Krommer, M. (2013), "Experimental static response characteristics of piezoceramic d_{15} shear-induced torsion sensing and actuation mechanisms", *Sens. Actuat. A- Phys*., Submitted.

Chopra, I. (2002), "Review of state of art of smart structures and integrated systems", *AIAA J*., **40**(11), 2145-2158.

Choi, S.C., Park, J.S. and Kim, J.H. (2007), "Vibration control of pre–twisted rotating composite thin-walled beams with piezoelectric fiber composites", *J. Sound Vib*., **300**(1-2), 176-196.

Finio, B.M. and Wood, R.J. (2011), "Optimal energy density of piezoelectric twisting actuators", *Proceedings of the IEEE/RSJ Int. Conf. on Intelligent Robots and Systems*, San Francisco, USA, 25-30 September.

Hajianmaliki, M. and Qatu, M.S. (2013), "Vibrations of straight and curved composite beams: a review", *Compos. Struct*., **100**(6), 218-232.

Krommer, M., Berik, P. and Benjeddou, A. (2013), "Exact 3D Saint–Venant type solutions for piezoelectric d_{15} shear-mode bi-morph and sandwich torsion actuation and sensing problems", *Acta Mech.*, **224**(11), 2505-2527.

Krommer, M., Berik, P., Vetyukov, Y. and Benjeddou, A. (2012), "Piezoelectric d_{15} shear response–based torsion actuation mechanism: an exact 3D Saint–Venant type solution", *Int. J. Smart Nano Mater.*, **3**(2), 82-102.

Li, H., Hu, S.D., Tzou, H.S. and Chen, Z.B. (2012), "Optimal vibration control of conical shells with collocated helical sensor/actuator pairs", *J. Theor. Appl. Mech*., **50**(3), 769-784.

Niezrecki, C., Brei, D., Balakrishnan, S and Moskalik, A. (2001), "Piezoelectric actuation: state of art", *Shock Vib.*, **33**(4), 269-280.

Nin, A. and Abramovich, H. (2010), "Design, analysis and testing of a smart fin", *Compos. Struct.*, **92**, 863-872.

Pan, C.L. Ma, Y.T., Liu, Y.B., Zhang, Q. and Feng, Z.H. (2008), "Torsional displacement of piezoelectric fiber actuators with helical electrodes", *Sens. Actuat. A- Phys.*, **148**(1), 250-258.

Tzou, H.S., Ye, R. and Ding J.H. (2001), "A new X-actuator design for dual bending/twisting control of wings", *J. Sound Vib*., **241**(2), 271-281.

Yocum, M. and Abramovich, H. (2002), "Static behavior of piezoelectric actuated beams", *Comput. Struct*., **80**, 1797-1808.

Zehetner, C., Zellhofer, Krommer, M. and Brandl, A. (2012), "Control of torsional rod vibrations by piezoelectric transducers", *Proceedings of the 7th Int. Conf. on Computational Mechanics for Spatial Structures*, Sarajevo, Bosnia & Herzegovina, 2-4 April.

Appendix

The smart sandwich beam benchmark piezoelectric and composite materials properties are recalled in Table 5 from Berik and Benjeddou (2011). Note that both materials are transverse-isotropic but have isotropy in different planes: material plane 1-2 for the piezoceramic and 2-3 for the glass fiber/epoxy composite. Besides, for activating the shear-induced torsion actuation mechanism using these data, the *axially polarized* piezoceramic patches should have their material axis 1 (polarization direction) lying geometrically along the axis of the beam.

Table 5 Material properties of the sandwich beam core PZT PIC255 patches and the glass fiber/epoxy composite faces

Materials	Constants	Notations	Values
PIC255	Piezoelectric coupling	$e_{15} = e_{24}$	11.9
Axially polarized	*stress* constants (C/m^2)	$e_{31} = e_{32}$	-7.15
		e_{33}	13.7
	Dielectric constants at constant *strain* (nF/m)	$\in_{22}^{S}=\in_{33}^{S}$	8.234
		$\in_{11}^{S}$	7.588
	Young's moduli (GN/m^2)	$E_2 = E_3$	62.89
		E_1	47.69
	Shear moduli (GN/m^2)	$G_{13} = G_{12}$	22.26
		G_{23}	23.15
	Poisson's ratios	$\nu_{13} = \nu_{12}$	0.46
		ν_{23}	0.36
	Mass density (kg/m^3)	ρ	7800
Glass fiber/epoxy	Young's moduli (GN/m^2)	$E_2 = E_3$	13.1
		E_1	33.11
	Shear Moduli (GN/m^2)	$G_{13} = G_{12}$	3
		G_{23}	2.3
	Poisson's ratios	$\nu_{13} = \nu_{12}$	0.27
		ν_{23}	0.4
	Mass density (kg/m^3)	ρ	2620